Fermi Rubik's Cube in High-Pressure Induced Chlorine-Rich Compounds

Jun Kong(孔君)[1,2], Lei Su(苏磊)[2,3], Haixu Cui(崔海旭)[4], Hairui Ding(丁海芮)[1], Jingyu Hou(侯晶钰)[1], Chunxia Chi(迟春霞)[1], Shiyang Liu(刘诗洋)[1], Xiang-Feng Zhou(周向锋)[5], Hui-Tian Wang(王慧田)[6], and Xiao Dong(董校)[1*]

[1]*Key Laboratory of Weak-Light Nonlinear Photonics and School of Physics, Nankai University, Tianjin 300071, China*
[2]*Center for High Pressure Science and Technology Advanced Research, Beijing 100093, China*
[3]*Key Laboratory of Photochemistry, Institute of Chemistry, University of Chinese Academy of Sciences, Chinese Academy of Sciences, Beijing 100190, China*
[4]*College of Physics and Materials Science, Tianjin Normal University, Tianjin 300387, China*
[5]*Center for High Pressure Science, State Key Laboratory of Metastable Materials Science and Technology, School of Science, Yanshan University, Qinhuangdao 066004, China*
[6]*National Laboratory of Solid State Microstructures, School of Physics, and Collaborative Innovation Center of Advanced Microstructures, Nanjing University, Nanjing 210093, China*

(Received 11 August 2024; accepted manuscript online 9 September 2024)

In the quasi-free electron model, the Fermi surface spreads into a sphere in the Brillouin zone, i.e., the Fermi sphere. The Fermi sphere exists widely in metal systems, no matter whether the crystal is in a body-center cubic, face-center cubic, or hexagonal close-packed lattice. Here, we report a class of compounds stabilized at high pressure with Rubik's cubic Fermi surface, in which the representative example is $Pm\bar{3}n$-$CaCl_3$. Our quantum-mechanical variable-composition evolutionary simulations predict the thermal stabilities of $CaCl_3$, and the tight-binding model reveals that its unique Fermi surface originates from the quasi-one-dimensional interaction, structural symmetric protection, and particle-hole symmetry breaking. Furthermore, by its flat and steep band structure, $CaCl_3$ has a huge span of effective mass from $9.08 \times 10^3 m_e$ (super-heavy) to $5.13 \times 10^{-4} m_e$ on the Fermi level, which supplies an interesting platform for quasiparticle research.

DOI: 10.1088/0256-307X/41/10/107101

The concept of Fermi surface is very crucial to our understanding of metallic states, which in reciprocal space ($\boldsymbol{k}$-space) separates the occupied from the unoccupied electron states at 0 K. The dynamical properties of an electron on the Fermi surface depend on its placement on the Fermi surface. The shape of the Fermi surface to the Brillouin zone can give information about the electrical properties of a metal. The Fermi surface plays an important role in various scientific phenomena, including oscillations of exchange coupling,[1,2] shape memory,[3,4] and superconductivity.[5–7] Plenty of the discussion has centered on understanding the phenomena resulting from the topology of the Fermi surface.[8] Most scholars first encounter Fermi surfaces through the Sommerfeld free electron model, in which it has a spherical shape, and the energy of the single-electron state on the Fermi surface is called the Fermi energy, which is $E_{\boldsymbol{k}} = \hbar^2\boldsymbol{k}^2/2m$, where $\boldsymbol{k}$ is the momentum of the electron. In real metals, the Fermi surface might differ significantly from a sphere.[9] Scientists have found that some metals have multiple disconnected Fermi surfaces, which are also known as pockets or valleys.[8,10] However, the shapes of Fermi surfaces, other than spheres (which are found in a free electron gas) and pockets (which are found in topological materials and semimetals), have not been discussed so much by scientists. These shapes are very important and can even determine the electronic properties of a material. Here, by quantum-mechanical variable-composition evolutionary simulations, we predict a thermal stable phase in the Ca–Cl system and find that it has Rubik's cubic Fermi surface, which has never been reported before to our knowledge.

Calcium compounds have important scientific value in biomineralization and geosciences, while chlorine is widely present in nature and used in the industrial production of plastics. In addition, chloride salts with the Cl^- anion contribute about 2% of the oceans' mass. NaCl, the most familiar of these chloride salts, exhibits highly unusual properties under high pressure. At high pressure, new materials with different stoichiometries emerge in the Na–Cl system.[11] These structures exhibit exotic electronic properties, especially for compounds in the Cl-rich edge ($Na:Cl > 1$). These works have further gone on to stimulate research into other binary or ternary systems at high pressure to investigate unusual chemical compositions.[12–19] Some of these compounds reveal a new class of Cl-rich compounds with extra-high coordination numbers up to 12, which are only induced under high pressures and possibly contain new electronic phenomena.

Considering the intriguing stoichiometries, structures, and electronic properties of Cl-related substances under

*Corresponding author. Email: xiao.dong@nankai.edu.cn
© 2024 Chinese Physical Society and IOP Publishing Ltd

compression, binary bulk compounds formed by Ca and Cl atoms may show more fantastic high-pressure behaviors. In this work, we theoretically study and discover a high-pressure metallic phase of $CaCl_3$ containing unusual Cl chains. To investigate the electronic properties and chemical bonding of $CaCl_3$, we calculate the electron localization function (ELF),[20] electronic band structure, density of states (DOS), Bader charges,[21] and Fermi surface, which show a lot of rich and interesting properties. In addition, the electronic band structure and Rubik's cubic Fermi surface structure are analyzed using the tight-binding model.

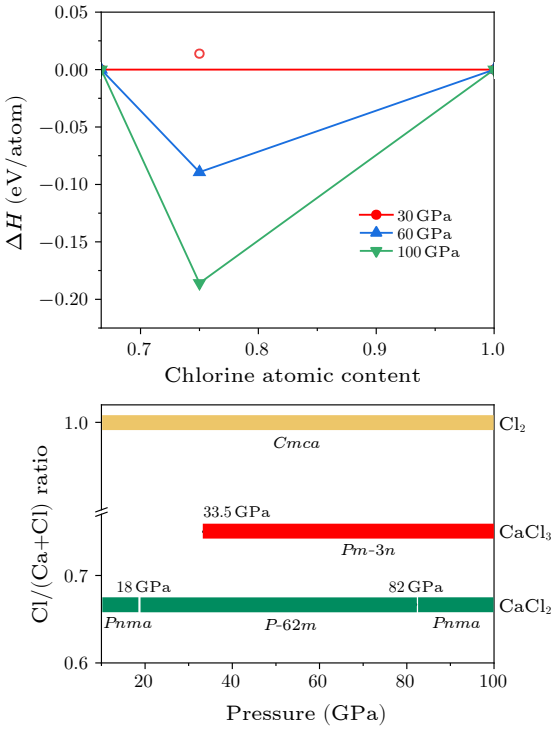

Fig. 1. Stability of new calcium chlorides. (a) Convex hull for the $CaCl_2$–Cl system at selected pressures. Solid symbols represent stable compounds; open symbols denote metastable compounds. ΔH represents the enthalpy of formation per atom. (b) Pressure-composition phase diagram of the $CaCl_2$–Cl system.

Our extensive search for calcium-chlorine system crystal structures considered pressures of 0, 30, 60, and 100 GPa using the USPEX code,[22,23] which can efficiently find stable structures given only the chemical composition. In this work, we mainly focus on chlorine-rich compounds. The candidate structure was relaxed using the VASP code,[24–26] and its thermodynamic stability was systematically investigated by calculating the formation enthalpies relative to $CaCl_2$ and Cl at the corresponding pressure. The formation enthalpy per atom in Ca_xCl_y is defined as

$$\Delta H = [H(Ca_xCl_y) - xH(CaCl_2) - (y-2x)H(Cl)]/(x+y), \quad (1)$$

where ΔH is the formation enthalpy per atom, and H is the calculated enthalpy of each compound. We restricted ourselves to ground state calculations, i.e., $H = E + PV$. If the formation enthalpy of a compound was negative, this compound was considered to be stable with respect to decomposition into $CaCl_2$ and Cl. To account for all possible compounds, we constructed the "convex hull" or "global stability line" of all considered binary phases. In such a phase diagram, where ΔH is plotted versus the chloride content, all points on the convex hull were stable against all decompression reactions. The convex hull for the Ca–Cl system of the Cl-rich regime is displayed in Fig. 1(a), and detailed enthalpy calculations for the most stable structures allowed us to construct the pressure-composition diagram of the Cl-rich regime of the Ca–Cl system [Fig. 1(b)], which provides potentially useful information for experimental synthesis.

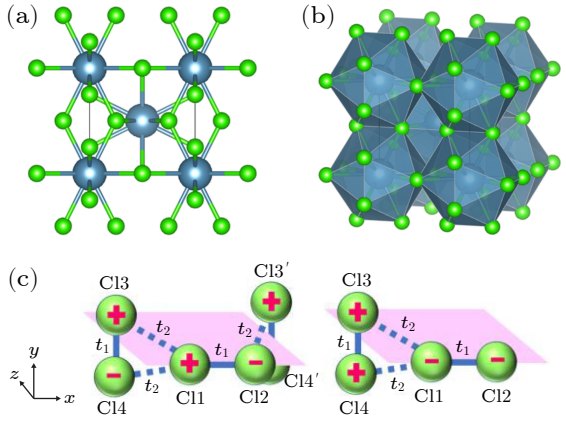

Fig. 2. Crystal structures of $Pm\bar{3}n$-$CaCl_3$ optimized at 50 GPa. (a) View down the c-axis. (b) Cl atoms form the Cl_{12} icosahedra. Blue and green spheres denote Ca and Cl atoms, respectively. (c) The schematic diagram of Cl1, Cl2, Cl3, and Cl4 interactions [$t_1 = 2.45$ eV and $t_2 = 0.1$ eV at 50 GPa in Eq. (2), which denote the hopping integral between the nearest neighbor or next-nearest neighbor orbitals, respectively]. Plus and minus signs correspond to the phase of projection of the Cl atom wave function. The red plane is the x–z plane, which is the symmetrical mirror of the structure. Crystal structures were drawn using VESTA software.[27]

The pressure-composition phase diagram predicted in our calculations contains a new stable compound, $CaCl_3$, with the same structure as $NaCl_3$.[11] We found that $CaCl_3$ is thermodynamically stable at high pressure [Fig. 1(b)], which is always located on the convex hull line from 33.5 GPa to at least 100 GPa. This stable compound has lower free energy than any iso-chemical mixture of other compounds or pure elements, indicating that it does not decompose into monomers and other compounds thermodynamically. As shown in Figs. 1(b), 2(a), and 2(b), $CaCl_3$ stabilized in a metallic A15 (Cr_3Si-type) structure with space group $Pm\bar{3}n$ at 33.5 GPa from our calculations. Crystallographic information of the stable phase $CaCl_3$ is summarized in Table S1. Phonon calculations[28] for $CaCl_3$ at pressures (above 1 GPa) of its stability show that no imaginary phonon frequencies exit throughout the Brillouin zone (see Fig. S1 in the Supplementary Material), suggesting that $Pm\bar{3}n$-$CaCl_3$ is dynamically stable. To in-

vestigate the nature of its stability, especially on the commonness and differences between $CaCl_3$ and $NaCl_3$, we analyzed the chemical bonding and electronic structures for $Pm\bar{3}n$-$CaCl_3$.

The shortest Cl–Cl distance (inner-chain) in $CaCl_3$ is 2.27 Å at 100 GPa, slightly longer than the Cl–Cl bond in the Cl_2 molecule (1.99 Å). These Cl–Cl bonds form extended monatomic chains running along three mutually perpendicular axes and we show the schematic diagram of interactions between Cl atoms in Fig. 2(c). This is very familiar with $Pm\bar{3}n$-$NaCl_3$,[11] which is reported to have 2.06 Å of Cl–Cl at 200 GPa. There are three mutually perpendicular chlorine chains arranged in the structure. This linear chain with a partially filled band is a textbook model. An isolated Cl chain with the unfilled band would break into Cl_2 molecules by Peierls instability,[29] but the application of pressure and the interaction among Cl chains stabilized these chains in $CaCl_3$ and $NaCl_3$.

To reveal the valence of Ca in $CaCl_3$, we computed Bader charges[21] of Ca and Cl atoms (see Table S1 in the Supplementary Material). The Bader charges of the Ca atoms are 1.45 in $CaCl_3$, similar to 1.38–1.42 in $CaCl_2$ at 50 GPa, implying that Ca in $CaCl_3$ is close to the classical divalent state in $CaCl_2$. Note that it is a common phenomenon that Bader charges are smaller than its valence, because there is a little component of covalent bonds between the cations and anions, i.e., incomplete ionization.

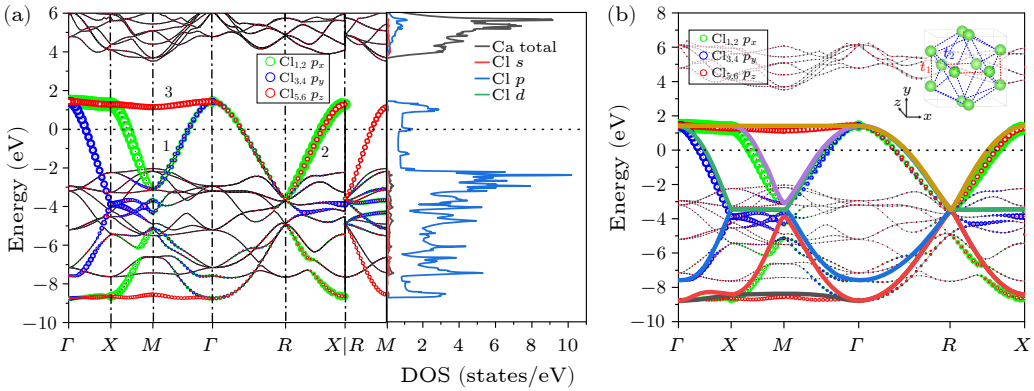

Fig. 3. Electronic structures of $Pm\bar{3}n$-$CaCl_3$ at 50 GPa. (a) The electronic projected band structure on designated atoms (fatband plot) and projected density of states on each element of $CaCl_3$ at 50 GPa. The width of the points indicates the weight of the designated atoms' contribution. (b) The energy band structures from the tight-binding model (solid thick lines) and density functional theory (DFT) calculations. Inset picture: the crystal structure only shows chlorine atoms and electron hopping integrals (t_1 and t_2) between chlorine atoms. The t_1 is shown by a red dashed line and the t_2 is shown with a blue dashed line.

Figure 3(a) shows the projected electronic band structure and projected density of states (PDOS) of $CaCl_3$ at 50 GPa. Figure 3(b) shows the energy band structures from the tight-binding model and density functional theory (DFT) calculations. The projected density of states in Fig. 3(a) shows that the density of states near the Fermi level is dominated by the p electronic states of the metallic Cl chains. The electron localization function shows asymmetry between the Ca and Cl atoms with most valence electrons localizing around Cl atoms, indicating the ionization of the Ca–Cl bonds and covalence of the Cl–Cl bonds (Fig. S2). In this structure, Cl atoms forming the Cl_{12} icosahedra show toroidal electron localization function maxima corresponding to a non-closed-shell electronic configuration, just like in $NaCl_3$.[11] By the divalent state of Ca and metallic Cl–Cl bonds, $CaCl_3$ has a band structure like p-type doping, i.e., the Fermi level is in its valence band (1.42 eV below the top of the band at 50 GPa). $NaCl_3$ is similar, but its Fermi level is much deeper than $CaCl_3$ (3.51 eV below the band top at 50 GPa) by one more electron lost.

Further insight is provided by calculating the Fermi surface of $Pm\bar{3}n$-$CaCl_3$ to learn more about its structural and unique electronic properties. The Fermi surface of the $Pm\bar{3}n$-$CaCl_3$ is shown in Fig. 4. As shown in Fig. 3(a), three energy bands are going through the Fermi level, among which the band from the $Cl_{5,6}p_z$ orbital has a flat band in the path of Γ–X–M–Γ. This flat band has a bandwidth of 290 meV in the path of Γ–X–M–Γ. The iso-energy surfaces near the Fermi level of these three bands are shown in Fig. S3. The flat band crosses the M point of the first Brillouin zone at $E = 1.2$ eV [Figs. 3(a) and S3]. Interestingly, the iso-energy surface of the flat band forms the patterns of Christmas stars on the six faces of the cubic Brillouin zone, and this iso-energy surface exhibits nesting along the X–Γ direction (Fig. S3). All three bands cross the E_F along the Γ–R direction and exhibit Rubik's cubic Fermi surface topology. Three bands have shapes of a cube, cross square pipes, and cubes in the Brillouin zone corners. These three bands form a $3 \times 3 \times 3$ Rubik's cube in total, as shown in Fig. 4(d).

Having topological electronic flattened bands near the Fermi level is a promising path to unconventional superconductivity and related insulating states.[30] The presence of "flat band and steep band" characteristics and Fermi surface nesting behavior is favorable for achieving superconducting transitions.[31] However, $CaCl_3$ did not show an estimated superconducting transition by our cal-

culations using the Quantum Espresso,[32] like $NaCl_3$.

However, it is also important to discuss its flat and steep band around the Fermi level. Regnault *et al.* discussed a catalogue of naturally occurring three-dimensional stoichiometric materials with flat bands around the Fermi level.[30] Their study indicated that materials host line-graph or bipartite sublattices, in either two or three dimensions, which probably lead to flat bands. Specifically, the flatness of bands of $RbMo_3S_3$ at the Fermi level is due to the weak inter-chain coupling of the quasi-one-dimensional crystal structure. Similar to $RbMo_3S_3$, $CaCl_3$ has three cross Cl chains in its structure, but these three chains have strong interactions with the nearest interchain atomic distance of 2.95 Å, which is only slightly larger than the distance of the nearest intrachain Cl atoms (2.32 Å), i.e., the shortest Cl–Cl bonds.

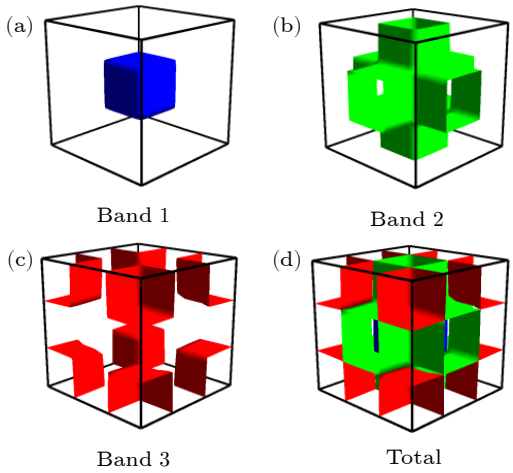

Fig. 4. Fermi surface of the $Pm\bar{3}n$-$CaCl_3$ structure. There are three energy bands [(a), (b), (c)] through the Fermi energy. (d) A total view.

To explore the origin of the flat and steep band and its strange Rubik's cubic Fermi surface, we used the tight-binding (TB) model to study the band structure near the Fermi level of $CaCl_3$. As shown in Fig. 2(c), the hopping integral of nearest neighbor (intrachain) and next-nearest neighbor (interchain) sites are set as t_1 and t_2, and the simplified TB Hamiltonian can be written in second quantization form as

$$\begin{aligned} H &= \sum\nolimits_{\langle i,j\rangle} t_{i,j} a_i^\dagger b_j + \text{H.c.} \\ &= T_1 \sum\nolimits_{\langle i,j\rangle_1} a_i^\dagger b_j + t_2 \sum\nolimits_{\langle i,j\rangle_2} a_i^\dagger b_j + \text{H.c.} \\ &= -t_1 \sum\nolimits_{\langle i,j\rangle_1} a_i^\dagger b_j + t_2 \sum\nolimits_{\langle i,j\rangle_2} a_i^\dagger b_j + \text{H.c.} \end{aligned} \tag{2}$$

according to the geometry of the $CaCl_3$ structure, where the notations $a_i^\dagger$ and b_j represent the electron creation and annihilation operators at sites i and j, respectively, while $t_{i,j}$ denotes the hopping integral between the nearest neighbor or next-nearest neighbor orbitals. T_1 represents the hopping integral between the nearest neighbor sites, which is the electron intrachain hopping between Cl atoms, and $T_1 < 0$ is obtained from the parity and phase properties of the p orbital electrons and the spatial geometry of the σ bonds. If $t_1 = -T_1$, then $t_1 > 0$. Here, t_2 represents the hopping integral between the next-nearest neighbor sites, an electron interchain hopping between Cl atoms, which could be positive or negative.

We chose the p_x orbits ($P_{1,x}$, $P_{2,x}$) of atoms 1 and 2, the p_y orbits ($P_{3,y}$, $P_{4,y}$) of atoms 3 and 4, and the p_z orbits ($P_{5,z}$, $P_{6,z}$) of atoms 5 and 6 as the atomic orbital basis vectors according to the fatband [Fig. 3(a)]. These six orbitals have the same axes with the extension directions of the chains of atoms. Therefore, the above Hamiltonian is converted into a 6×6 matrix, as shown in Eq. (S1) in the Supplementary Material.

For a simple case, we set $t_2 = 0$ to ignore the interchain interaction. The system degrades into three independent one-dimensional Cl chains, and the solution (eigenvalues) of the Hamiltonian is $E_{1\sim6} = \pm 2t_1 \cos[(a/2)k_i]$ ($i = x$, y, z), as shown in Fig. S4(b). In this simple case, the system has particle-hole symmetry, i.e., the upper three bands are the same as the lower three bands with a "mirror" symmetry in energy space. Bands are flat for every section parallel to the face of the cubic Brillouin zone. The iso-energy surface of $k_i = \pm(2/a)\arccos(E/2t_1)$ ($i = x$, y, z) is an ideal $3 \times 3 \times 3$ Rubik's cube by its one-dimensional configuration. At the Γ point ($k_x = k_y = k_z = 0$), the wave functions are divided into two sets of triple degenerate states, $E = \pm 2t_1$, corresponding to two sets of three symmetrical wave functions and three anti-symmetrical wave functions as shown in Eqs. (S3) and (S4). The Γ point is also a van Hove singularity in this independent Cl chains model, corresponding to the calculated electronic density of states for peaks at $E = 0.98$ eV above the Fermi level (E_F) in actual $CaCl_3$, as shown in Fig. 3(a).

Then, we considered the situation of $t_2 \neq 0$, i.e., a considerable interchain interaction [Fig. S4(c)]. Initially, we focused on the Γ point with complete crystal symmetry, where the structure is fully protected by the mirror symmetry of the x–z, y–z, and x–y planes. The effects of t_2 break the particle-hole symmetry. For the symmetric wave function, the phases of two interchain Cl atoms have two choices: the same or opposite, corresponding to the concentration or repulsion interaction among chains, respectively. Therefore, the lower three bands with symmetric wave functions split into a double degenerate energy level ($-2t_1 - 4t_2$) (same phase between interchain atoms) and a non-degenerate energy level ($-2t_1 + 8t_2$) (opposite phase between interchain atoms), with an energy splitting of $12t_2$. However, for the anti-symmetrical wave function, another picture appears. They are equivalent regardless of whether the phases of the interchain are the same or opposite because one chooses the same phases in this edge and it should be opposite phases in the other edge. This is protected by the crystal mirror symmetries. Thus, the upper three bands remain triple degenerate with the energy of $2t_1$ at the Γ point. We mainly focused on the upper three bands below because the Fermi level of $CaCl_3$ is close to the top of the bands.

Away from the Γ point, the symmetrical protection cannot be completely satisfied, and the triple degenerate bands split into several situations:

(1) $k_i = 0$, ($i = x$, y, z), the midsection of the cubic Brillouin zone. By Eq. (S8), there is always one eigenvalue of $E_i = 2t_1$, ($i = 1,\ 2,\ 3$), which is the origin of the flat band in the path of Γ–X–M–Γ. Specifically, on the line of Γ–X ($k_y = k_z = 0$), two eigenvalues are fixed as $E_1 = E_2 = 2t_1$ and the flat band is double degenerate.

(2) $k_i = \pi/a$, ($i = x$, y, z), boundary faces of Brillouin cube. The R point ($k_x = k_y = k_z = \pi/a$) is quite special with six bands degenerating to the zero point of all six orbitals [Fig. S4(c)]. This is different from the actual situation (DFT), where the hybridization of other orbitals splits them into three groups of levels at this point. However, it does not affect our major conclusion because we only focus on the upper three bands. In the TB model, the iso-energy surface intersects with the boundary face to form a pattern of a cross, slightly different from the Christmas star in the actual $CaCl_3$, owing to the higher order of hopping in the actual situation.

(3) $k_i = k_j$, (i, $j = x$, y, z), diagonal sections of the Brillouin cube. Considering $k_y = k_z$, this section contains R, X, and Γ points. In the line of R–Γ, the original triple degenerate bands (when $t_2 = 0$) split into a group of double degenerate bands and one separated band ($2+1$) with very little splitting energy, and the maxima of splitting energy are about 0.15 eV in the TB model and 0.18 eV in the DFT calculation at 50 GPa. Except for the points on the Γ–R–X–Γ line, which have $2+1$ degeneracy, the other points on the diagonal sections have three splitting bands ($1+1+1$ degeneracy), but the splitting energy is limited by the high symmetry of cubic crystals.

(4) Other points in the Brillouin zone. Except for the above sections and faces, the other points have three splitting bands.

The effect of the interchain interaction on the Fermi surface is shown in Fig. S5, which deviates from the model of independent chains. Its main effect is to turn the sharp corners into rounded corners. Additionally, it opens several narrow and flat Fermi pockets [red and green lines in Fig. S5(d)] in the original degenerate region (near the $k_x = k_y$ surface) or forms a small gap [green and blue lines in Fig. S5(d)]. However, the difference in the Fermi surface is very small compared to the one-dimensional case where only the intrachain interactions are considered, and the Fermi surface exhibits a cubic symmetry and has a global Rubik's cube structure.

In general, the upper three bands deviate from the situation of independent chains ($t_2 = 0$) quite little and perform as one-dimensional structures owing to the antisymmetrical wave function and the cubic crystal symmetry. Specifically, similarity increases when the energy approaches $2t_1$. That is the origin of this strange Rubik's cubic Fermi surface topology of $CaCl_3$.

As reported by Zhang *et al.*,[11] $NaCl_3$ has the same structure and a similar band structure as $CaCl_3$. However, by two lost electrons in the primitive cell, the Fermi level of $NaCl_3$ is much lower than $CaCl_3$ and goes into the energy range of the lower three bands in the TB model. By breaking the particle-hole symmetry, the lower three bands are affected by the interchain interactions very much and veer away from the independent chain model. Therefore, only $CaCl_3$ has Rubik's cubic Fermi surface and $NaCl_3$ does not.

A flat and steep band structure or Fermi level usually means that there is an extreme value of effective mass.[30] A flat band means a very high effective mass up to infinity, while a steep band equates to a very low effective mass down to zero. For $CaCl_3$, the maximum mean effective mass is $8207.44m_e$ and $9078.02m_e$ (more than 10 times typical heavy fermion materials,[33] and much higher than magic-angle graphene, which is $0.05m_e$–$2m_e$,[34,35] where m_e is the bare electron mass) for the TB model and DFT, respectively. Meanwhile, the minimum mass is $4.59 \times 10^{-4} m_e$ and $5.13 \times 10^{-4} m_e$ for the TB model and DFT, respectively, which has a huge span in their values.

In summary, by structure prediction and *ab initio* calculations, we predict stable chlorine-rich compounds of $CaCl_3$ in the calcium-chlorine system, which form thermodynamically at 33.5 GPa and stabilize up to 100 GPa. We use calculated Cl–Cl bond lengths, band structure, Bader charges, and other electronic structures to explore the electronic properties and chemical bonding of $CaCl_3$ and find that it has Rubik's cube Fermi surface, quite different from the Fermi sphere in common metal. The TB model is used to explain the origin of this flat and steep band and Rubik's cubic Fermi surface, revealing that this strange Fermi surface shape is due to the quasi-one-dimensional nearest interaction. A higher order of interchain interaction breaks the particle-hole symmetry and is offset by the crystal symmetry and wave function phase. Our calculations on $CaCl_3$ discover a new class of materials with a special, flat, and steep shape of the energy band, supplying a new platform to research the strange electronic behavior of electrons, and providing a special insight into the band theory, especially for the flat bands and steep bands.

Acknowledgements. This work was supported by the Fundamental Research Funds for the Central Universities (Grant No. 010-63243095), the National Science Foundation of China (Grant Nos. 92263101 and 12174200). The calculations were performed and supported by Tianhe Ⅱ in Guangzhou and Supercomputing Center of Nankai University (NKSC).

References

[1] Parkin S S P, Farrow R F C, Marks R F, Cebollada A, Harp G R, and Savoy R J 1994 *Phys. Rev. Lett.* **72** 3718
[2] Hughes R J, Dugdale S B, Major Z, Alam M A, Jarlborg T, Bruno E, and Ginatempo B 2004 *Phys. Rev. B* **69** 174406
[3] McDonald R D, Singleton J, Goddard P A, Drymiotis F, Harrison N, Harima H, Suzuki M T, Saxena A, Darling T, Migliori A, Smith J L, and Lashley J C 2005 *J. Phys.: Condens. Matter* **17** L69
[4] Dugdale S B, Watts R J, Laverock J, Major Z, Alam M A, Samsel-Czekała M, Kontrym-Sznajd G, Sakurai Y, Itou M, and Fort D 2006 *Phys. Rev. Lett.* **96** 046406
[5] Yokoya T, Kiss T, Chainani A, Shin S, Nohara M, and Takagi H 2001 *Science* **294** 2518
[6] Sandeman K G, Lonzarich G G, and Schofield A J 2003 *Phys. Rev. Lett.* **90** 167005

[7] Sugawara K, Sato T, and Takahashi T 2009 *Nat. Phys.* **5** 40
[8] Alexandradinata A and Glazman L 2023 *Annu. Rev. Condens. Matter Phys.* **14** 261
[9] Kaganov M I and Lifshits I M 1979 *Sov. Phys. Usp.* **22** 904
[10] Guo C, Alexandradinata A, Putzke C, Estry A, Tu T, Kumar N, Fan F R, Zhang S, Wu Q, Yazyev O V, Shirer K R, Bachmann M D, Peng H, Bauer E D, Ronning F, Sun Y, Shekhar C, Felser C, and Moll P J W 2021 *Nat. Commun.* **12** 6213
[11] Zhang W, Oganov A R, Goncharov A F, Zhu Q, Boulfelfel S E, Lyakhov A O, Stavrou E, Somayazulu M, Prakapenka V B, and Konôpková Z 2013 *Science* **342** 1502
[12] Li Y L, Wang S N, Oganov A R, Gou H, Smith J S, and Strobel T A 2015 *Nat. Commun.* **6** 6974
[13] Li D, Tian F, Lv Y, Wei S, Duan D, Liu B, and Cui T 2017 *J. Phys. Chem. C* **121** 1515
[14] Yang L, Zhang Y, Chen Y, Zhong X, Wang D, Lang J, Qu X, and Yang J 2021 *Materials* **14** 7650
[15] Zhang W, Oganov A R, Zhu Q, Lobanov S S, Stavrou E, and Goncharov A F 2016 *Sci. Rep.* **6** 26265
[16] Zhang L, Shi G, Peng B, Gao P, Chen L, Zhong N, Mu L, Zhang L, Zhang P, Gou L, Zhao Y, Liang S, Jiang J, Zhang Z, Ren H, Lei X, Yi R, Qiu Y, Zhang Y, Liu X, Wu M, Yan L, Duan C, Zhang S, and Fang H 2021 *Natl. Sci. Rev.* **8** nwaa274
[17] Liu C, Wang J, Deng X, Wang X, Pickard C J, Helled R, Wu Z, Wang H T, Xing D, and Sun J 2022 *Chin. Phys. Lett.* **39** 076101
[18] Xie F, Lu T, Yu Z, Wang Y, Wang Z, Meng S, and Liu M 2023 *Chin. Phys. Lett.* **40** 057401
[19] Liu Y X, Wang C, Han S, Chen X, Sun H R, and Liu X B 2021 *Chin. Phys. Lett.* **38** 036201
[20] Becke A D and Edgecombe K E 1990 *J. Chem. Phys.* **92** 5397
[21] Henkelman G, Arnaldsson A, and Jónsson H 2006 *Comput. Mater. Sci* **36** 354
[22] Lyakhov A O, Oganov A R, Stokes H T, and Zhu Q 2013 *Comput. Phys. Commun.* **184** 1172
[23] Bushlanov P V, Blatov V A, and Oganov A R 2019 *Comput. Phys. Commun.* **236** 1
[24] Kresse G and Furthmüller J 1996 *Comput. Mater. Sci.* **6** 15
[25] Perdew J P, Burke K, and Ernzerhof M 1996 *Phys. Rev. Lett.* **77** 3865
[26] Blöchl P E 1994 *Phys. Rev. B* **50** 17953
[27] Momma K and Izumi F 2011 *J. Appl. Crystallogr.* **44** 1272
[28] Togo A and Tanaka I 2015 *Scr. Mater.* **108** 1
[29] Peierls R 1991 *More Surprises in Theoretical Physics* (Princeton: Princeton University Press)
[30] Regnault N, Xu Y, Li M R, Ma D S, Jovanovic M, Yazdani A, Parkin S S P, Felser C, Schoop L M, Ong N P, Cava R J, Elcoro L, Song Z D, and Bernevig B A 2022 *Nature* **603** 824
[31] Simon A 1997 *Angew. Chem. Int. Ed.* **36** 1788
[32] Giannozzi P, Baroni S, Bonini N, Calandra M, Car R, Cavazzoni C, Ceresoli D, Chiarotti G L, Cococcioni M, Dabo I, Dal Corso A, de Gironcoli S, Fabris S, Fratesi G, Gebauer R, Gerstmann U, Gougoussis C, Kokalj A, Lazzeri M, Martin-Samos L, Marzari N, Mauri F, Mazzarello R, Paolini S, Pasquarello A, Paulatto L, Sbraccia C, Scandolo S, Sclauzero G, Seitsonen A P, Smogunov A, Umari P, and Wentzcovitch R M 2009 *J. Phys.: Condens. Matter* **21** 395502
[33] Degiorgi L 1999 *Rev. Mod. Phys.* **71** 687
[34] Cao Y, Fatemi V, Fang S, Watanabe K, Taniguchi T, Kaxiras E, and Jarillo-Herrero P 2018 *Nature* **556** 43
[35] Park J M, Cao Y, Watanabe K, Taniguchi T, and Jarillo-Herrero P 2021 *Nature* **590** 249